



1        **Spatial-temporal distribution, photoreactivity and environmental**  
2        **control of dissolved organic matter in the sea-surface microlayer of**  
3        **the eastern marginal seas of China**

4                      Lin Yang <sup>a</sup>, Jing Zhang <sup>a,c,\*</sup>, Anja Engel<sup>d</sup>, Gui-Peng Yang <sup>a,b,c,\*</sup>

5        <sup>a</sup> Frontiers Science Center for Deep Ocean Multispheres and Earth System, and Key Laboratory of  
6        Marine Chemistry Theory and Technology, Ministry of Education, Ocean University of China,  
7        Qingdao 266100, China

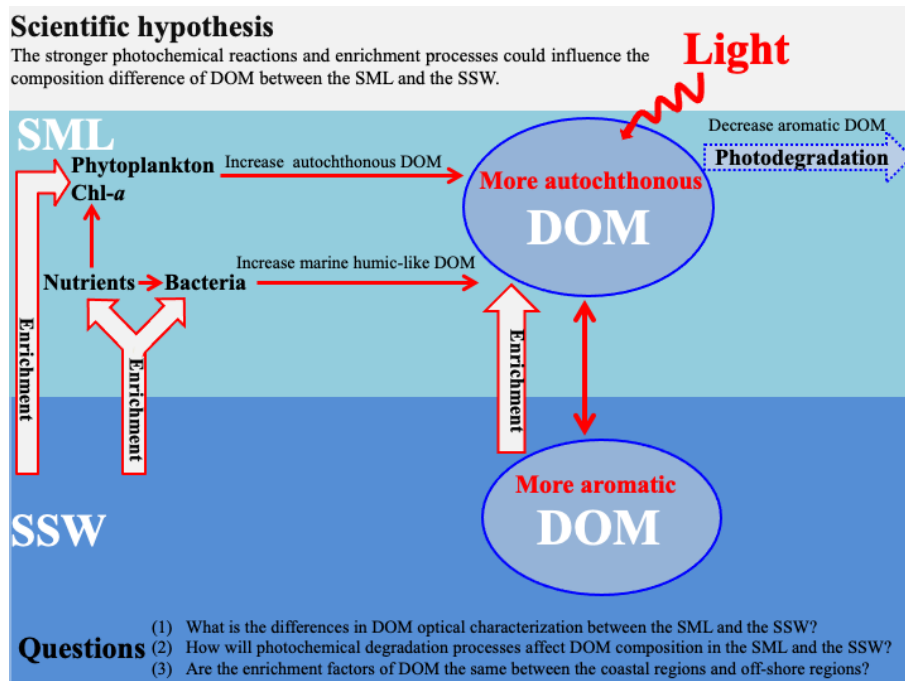
8        <sup>b</sup> Laboratory for Marine Ecology and Environmental Science, Qingdao National Laboratory for  
9        Marine Science and Technology, Qingdao 266237, China

10        <sup>c</sup> Institute of Marine Chemistry, Ocean University of China, Qingdao 266100, China

11        <sup>d</sup> GEOMAR Helmholtz Centre for Ocean Research, 24105 Kiel, Germany

---

\* Corresponding authors. Key Laboratory of Marine Chemistry Theory and Technology, Ministry of Education, Ocean University of China, Qingdao 266100, China  
E-mail addresses: [zhangjouc@ouc.edu.cn](mailto:zhangjouc@ouc.edu.cn) (J. Zhang), [gpyang@ouc.edu.cn](mailto:gpyang@ouc.edu.cn) (G.-P. Yang)



12

13

Graphical Abstract



14 **Abstract**

15 As the boundary interface between the atmosphere and ocean, the sea-surface microlayer (SML)  
16 plays a significant role in the biogeochemical cycles of dissolved organic matter (DOM) and  
17 macronutrients in marine environments. In our study, chromophoric DOM (CDOM), fluorescent DOM,  
18 dissolved organic carbon, chlorophyll *a*, picoplankton, nutrients, and bacteria were frequently enriched  
19 in the SML. We focus specifically on the optical properties in the SML, and we find that the  
20 enrichment factors (EFs) of tryptophan-like component 4 was significantly higher than other  
21 fluorescence components; the longer wavelength absorption values of CDOM showed higher EFs in  
22 the SML, and the more significant relationship between CDOM and Chl-*a* in the SML, indicating that  
23 autochthonous DOM was more frequently enriched in the SML than the terrestrial DOM. We find that  
24 higher EFs were generally observed in the SML in the off-shore regions than in the coastal regions,  
25 and CDOM in the SML is photobleached less after relatively strong irradiation, as also indicated by  
26 the lower percentages of humic-like DOM and lower specific UV absorbance values (SUVA<sub>254</sub>) in the  
27 SML than the subsurface water (SSW). In combination with the SSW, the elevated nutrients may  
28 stimulate phytoplankton growth, biological activity and then production of abundant fresh  
29 autochthonous DOM in the SML. Our results revealed a general enrichment model and the more  
30 autochthonous properties of DOM in the SML than the SSW for exploring the oceanic air-sea layer  
31 environment.

32

33 **Keywords:** Sea-surface microlayer; Dissolved organic matter; Photochemical degradation;  
34 Enrichment processes; Eastern marginal seas of China

35 **1 Introduction**



36 The sea-surface microlayer (SML) is the boundary interface between the atmosphere and the  
37 ocean, which covers about 70% of the Earth's surface. SML is physicochemically distinct from  
38 subsurface water (SSW, depth 3 ~ 5 m) and is characteristically enriched with phytoneston,  
39 chlorophyll, particulate carbon, dissolved organic matter (Hardy 1982; Hardy and Apts, 1989), and  
40 biogenic organic compounds, such as lipids, proteins, and polysaccharides ((Liss and Duce, 1997; Liss  
41 and Duce, 2005). With a total thickness ranging between 1  $\mu\text{m}$  and 1000  $\mu\text{m}$ , the SML remains present  
42 in wind speeds of up to 6.6  $\text{m s}^{-1}$  (Wurl et al., 2011). A variety of processes contribute to the formation  
43 of the SML in aquatic systems, these include but are not limited to, scavenging by rising bubbles,  
44 atmospheric deposition, dissolved organic matter (DOM) photochemical degradation and  
45 transformation, secretion, and biodegradation by organisms living within the microlayer (Neuston),  
46 and migration of motile organisms into the SML (Aller et al., 2005; Wotton and Preston, 2005). The  
47 role of the microlayer in oceanic emissions is not well understood and fundamental advance in  
48 understanding its properties are needed. Because of its unique position at the air-sea interface, the  
49 biological and photochemical reactions of DOM in the SML could strongly impact the biogeochemical  
50 cycling of biologically important elements, for example, via the conversion of DOM into volatile  
51 species such as carbonyl sulfide (OCS), which influence the atmospheric chemistry and climate  
52 (Mopper et al., 2002). Air-sea gas exchanges of trace gases (e.g., CO, OCS, dimethylsulfide (DMS),  
53 and alkyl nitrates gases) can also be greatly influenced by biological and photochemical reactions at  
54 the sea surface (Blough, 1997).

55 Optical measurements of absorbance and fluorescence have been applied to track DOM  
56 variability in aquatic ecosystems (McKnight et al., 2001; Zepp et al., 2004; Coble, 2007). The fraction  
57 of DOM that absorbs light in the ultraviolet and visible ranges of the electromagnetic spectrum and the



58 fraction that exhibits a blue fluorescence are known as chromophoric DOM (CDOM) and fluorescence  
59 DOM (FDOM), respectively, and their relative compositions can provide information differentiating  
60 between autochthonous and allochthonous sources (Coble, 1996; McKnight et al., 2001; Stedmon et  
61 al., 2007). Photolysis of DOM promotes the formation of low-molecular-weight compounds,  
62 increasing the bioavailability of biologically refractory materials and facilitating carbon uptake by  
63 microbes (Kieber et al., 1989). Indices based on optical measurements of absorbance and fluorescence  
64 are commonly used to track DOM composition and infer DOM processing due to their low analytical  
65 cost and high throughput relative to molecular level analyses (Coble, 2007; Fellman et al., 2010;  
66 Gabor et al., 2014). Recent studies have mainly focused on using the characteristics of CDOM as  
67 indicators of the sources and degradation states of DOM (Massicotte et al., 2017) in the SSW, and its  
68 vertical distribution in estuaries and open oceans (Yamashita et al., 2017; Margolin et al., 2018).

69 Even though there are many studies that have documented the enrichment in DOM (e.g. amino  
70 acids; carbohydrates) and inorganic nutrients in the SML relative to the SSW (Orellana et al., 2011;  
71 Chen et al., 2016), the differences in organic matter composition between the SML and SSW, the  
72 different enrichment factors of DOM in the SML between the coastal regions and the off-shore regions,  
73 and how do photochemical degradation activities regulate DOM concentration in the SML need more  
74 thorough discussion. Here, we investigated the concentration and composition of DOM in the SML  
75 relative to the SSW and the responses of DOM to photoexposure. We hypothesized that the  
76 photochemical reactions and enrichment processes could influence the composition difference of  
77 DOM between the SML and the SSW, and greater solar exposure in the SML than in the SSW would  
78 enhance the mineralization of DOM. To test these hypotheses, our study was designed to answer the  
79 questions: (1) What is the differences in optical characterization of DOM between the SML and the



80 SSW? (2) Are the enrichment factors (EFs) of DOM the same between the coastal regions and  
81 off-shore regions? (3) How will photochemical degradation processes affect DOM composition in the  
82 SML and the SSW? We, therefore, compared the optical properties of DOM between the SSW and the  
83 SML, and EFs of CDOM, FDOM components, dissolved organic carbon (DOC), chlorophyll-*a* (Chl-*a*),  
84 nutrients, and bacterial abundance from the coastal waters to open ocean in the eastern marginal seas  
85 of China (including the East China Sea (ECS) and the Yellow Sea (YS)) during spring of 2017 and  
86 2019, summer of 2018, and winter of 2019; discuss how the composition of accumulated DOM was  
87 affected by environmental conditions (wind speed and salinity) within the SML; and conducted  
88 photoexposure experiments to compare photochemical degradation processes of DOM between the  
89 SML and the SSW.

90

## 91 **2 Materials and methods**

### 92 *2.1 Study Area*

93 Five cruises were conducted during the four seasons, specifically, from: 27 March to 15 April  
94 2017 (R/V “*Dong Fang Hong 2*”), 26 June to 19 July 2018 (R/V “*Dong Fang Hong 2*”), March 2019  
95 (R/V “*Zheyu No. 2*”), and 28 December 2019 to 16 January 2020 (R/V “*Dong Fang Hong 3*”). The  
96 station locations are shown in Fig. S1. In spring, summer, and winter, SML samples were collected in  
97 the YS and the ECS, which are shallow seas located almost entirely on the continental shelf in the  
98 western Pacific Ocean where there is strong interaction between land and sea.

### 99 *2.2 Sampling*

100 We collected 220 paired SML and SSW water samples. SSW samples were collected at 2–5 m  
101 depth using 24 × 10-L Niskin bottles mounted on a rosette equipped with a



102 conductivity-temperature-depth (CTD) profiler. The SML samples were collected using the screen  
103 sampling technique (Chen et al., 2016; Garrett, 1965) when conditions were calm. A screen sampler  
104 with a 1.6 mm mesh of stainless steel wire on a 40 cm × 40 cm stainless steel frame was used. The  
105 SML samples were collected in 500 mL brown sample bottles. The screen was held level and dipped  
106 into the sea surface, moved laterally in order to sample from an undisturbed film, and then withdrawn  
107 slowly from the surface. Repeated dipping was conducted until the desired volume was collected. The  
108 screen method is often applied during field studies because of its relatively short sampling time and  
109 large sample volume compared to other techniques (Momzikoff et al., 2004; Chen et al., 2016).  
110 Immediately after collection, samples were filtered using 0.7 µm glass fiber filters (GF/F, Whatmann)  
111 and the filtrates were transferred to 60 mL and 40 mL brown glass bottles (pre-cleaned and  
112 pre-combusted) for later CDOM and DOC analyses. All samples were frozen (-20°C) and protected  
113 from light, and upon arriving at the land laboratory, were analyzed as soon as possible.

### 114 *2.3 Photoexposure experiment*

115 SSW and SML water samples were collected in July 2018 at stations A3, BF, and H10 as well as  
116 D2 and F6 located in the YS and the ECS, respectively. Samples (SSW: 2L; SML: 500 mL) were  
117 immediately passed through 0.22 µm PES filters (Pall Corp. Port Washington, NY, USA) to remove  
118 the majority of bacteria, placed in acid-washed and pre-combusted brown glass bottles and stored at  
119 4°C. Similarly, filtered samples from each site were placed in five 80 mL optically transparent quartz  
120 tubes (acid-washed and pre-combusted) and sealed without headspace or air bubbles to measure the  
121 effect of light exposure. The quartz tubes were positioned on their sides under the irradiation source to  
122 maximize the exposure of the sample; the water depth in each tube was 5 cm (i.e. the diameter of the  
123 tube). Both sets (SML and SSW) were irradiated for 6, 12, 24, 50, and 88 h (25°C) in a GLZ-C



124 Quantum Sensor (Top Cloud-Agri Instrument, Zhejiang, China) solar simulator. All samples for DOC  
125 concentration measurements were acidified to approximately pH 2.0 with high purity HCl and  
126 analyzed within 7 d, and absorbance spectra and fluorescence excitation emission matrices (EEMs)  
127 were run on non-acidified samples within 3 d of sampling (4°C and dark).

#### 128 *2.4 Analytical measurements*

##### 129 *Determination of the CDOM absorption coefficient*

130 Absorption spectra were determined using a UV-visible spectrophotometer (UV-2550 bi-channel;  
131 Shimadzu, Tokyo, Japan) equipped with two 10 cm path-length quartz cuvettes. Sample absorbance  
132 was automatically corrected for the absorbance of Milli-Q water. Absorbance scans ranged from 200 to  
133 800 nm, with a spectral resolution of 1 nm. The absorption coefficient of CDOM was calculated  
134 according to equation (1):

$$135 \quad a(\gamma) = 2.303A(\gamma)/l \quad (1)$$

136 where,  $A(\lambda)$  is the absorbance at wavelength  $\lambda$ ; and  $l$  is the path length of the quartz cuvette in meters.

137 The spectral slope of the CDOM absorption curve ( $S$ ) was calculated according to a non-linear  
138 regression over the 275–295 nm and 350–400 nm wavelength range, according to:

$$139 \quad a(\lambda) = a(\lambda_0)\exp[S(\lambda_0 - \lambda)] + K \quad (2)$$

140 where,  $a(\lambda)$  is the absorption coefficient at wavelength  $\lambda$ ;  $a(\lambda_0)$  is the absorption at the reference  
141 wavelength  $\lambda_0$  of 440 nm;  $S$  is the spectral slope; and  $K$  is a background parameter that accounts for  
142 baseline shifts or attenuation due to factors other than CDOM.  $S$  was measured in the wavelength  
143 ranges of 275–295 nm ( $S_{275-295}$ , nm<sup>-1</sup>) and 350–400 nm ( $S_{350-400}$ , nm<sup>-1</sup>).  $S_{275-295}$  is used to characterize  
144 DOM, with high values generally indicative of low-molecular-weight DOM that are linked to  
145 photochemical modification (Helms et al., 2008; Ortega-Retuerta et al., 2009). The spectral slope ratio  
146 ( $S_R$ ) was defined as the ratio of the two spectral slopes,  $S_{275-295}$  to  $S_{350-400}$ .  $S_R$  is also a sensitive  
147 indicator of photochemically induced changes in the molecular weight within the CDOM pool, with



148 increases in  $S_R$  suggesting stronger photochemical degradation (Helms et al., 2008; Ortega-Retuerta et  
149 al., 2009). We used the absorption coefficient at 254 nm ( $a(254)$ ) to determine the concentration and  
150 distribution of CDOM in the SML from the eastern marginal seas of China. The specific UV  
151 absorbance ( $SUVA_{254}$ ) can be used to measure aromaticity (Weishaar et al., 2003) and molecular  
152 weight (Chowdhury, 2013) of DOM, with higher values generally indicative of higher aromaticity.

153 *EEMs and determination of the CDOM fluorescence index*

154 EEMs were obtained using a F-4500 fluorescence spectrophotometer with a 1 cm quartz cuvette  
155 (Shimadzu) (Hoge et al., 1993). The emission spectra were scanned every 5 nm from 250 nm to 550  
156 nm, and at the excitation wavelengths between 200–400 nm at 5 nm intervals, with 5 nm slit widths  
157 for the excitation and emission modes. The FL Toolbox, which was developed by Wade Sheldon  
158 (University of Georgia) for MATLAB, was used to remove the Rayleigh and Raman scattering peaks  
159 using the Delaunay triangulation method (Zepp et al., 2004). The fluorescence intensities of the  
160 samples were corrected with Milli-Q water blank EEMs and then normalized to the water Raman  
161 integrated area maximum fluorescence intensities ( $Ex/Em = 350 \text{ nm}/365\text{--}430 \text{ nm}$ , 5 nm bandpass)  
162 (Coble et al., 1998; Singh et al., 2010). Raman units (RU) (Stedmon et al., 2007; Singh et al., 2010)  
163 were used as the units for the Raman peak areas of water when the excitation wavelength of 350 nm  
164 was used for correction. EEMs were modeled using PARAFAC in MATLAB 7.5 with the DOMFluor  
165 toolbox (Stedmon and Bro, 2008).

166 
$$X_{ijk} = \sum_{n=1}^F a_{in} b_{jn} c_{kn} + \varepsilon_{ijk} \quad (3)$$

167 where  $X_{ijk}$  is the fluorescence intensity of the  $i$ th sample at the  $k$ th excitation and  $j$ th emission  
168 wavelengths;  $a_{in}$  is directly proportional to the concentration (scores) of the  $n$ th fluorophore in the  $i$ th  
169 sample;  $b_{jn}$  and  $c_{kn}$  are the estimates of the emission and excitation spectra (loadings) of the  $n$ th  
170 fluorophore at wavelengths  $j$  and  $k$ , respectively;  $F$  is the number of components (fluorophores); and  
171  $\varepsilon_{ijk}$  represents the unexplained variability of the model (Singh et al., 2010). Split-half analysis  
172 validation was used to determine the number of fluorescent components. The fluorescence intensity of  
173 each fluorescent component was evaluated (Fig. S2, Supporting Information, Table 1).



174 *Determination of DOC, chlorophyll-a, heterotrophic bacterial abundance, dissolved oxygen, and*  
175 *other parameters*

176 Concentrations of DOC were determined using the Shimadzu TOC-V<sub>CPH</sub> total organic carbon  
177 analyzer with an injection volume of 80 µL. The accuracy of the test was ensured by measuring a deep  
178 seawater reference (Hansell Laboratory, University of Miami) every 10 samples. The Chl-*a*  
179 concentration was determined by a fluorescence spectrophotometer (7200-000, Turner Designs, CA)  
180 after extraction in 90% acetone based on the procedure of Parsons et al. (1984). DO was determined  
181 by iodination using the Winkler titration method (Carpenter, 1964), the endpoint was determined using  
182 starch as a visual indicator. Salinity and temperature data were collected in situ by a  
183 conductivity-temperature-depth sensor. All phytoplankton samples were enumerated in triplicate  
184 according to Specification for Oceanographic Survey (State Bureau of Technical Supervision Bureau,  
185 1992). Nutrient species concentrations were determined using an automatic analyzer (QuAatro, Seal  
186 Analytical, Germany) (Grasshoff et al., 2007). Heterotrophic bacterial abundances were measured by  
187 flow cytometry (colorimetry, Beckman Coulter FC500-MPL) as described by Marie et al. (1997).

188 *Enrichment factors*

189 The enrichment factor (EF) in the SML is defined as follows

$$190 \quad EF = C_M / C_S \quad (4)$$

191

192 where  $C_M$  is the concentration of any substance in the SML; and  $C_S$  is its concentration in the SSW. If  
193 the EF of a substance is greater than 1.0, that substance is considered enriched, if it is less than 1.0, it  
194 is considered depleted (Chen et al., 2016).

195 *2.5 Statistical analyses*



196 The correlation coefficient ( $R$ ) and probability ( $P$ ) values were used to evaluate the  
197 goodness-of-fit. The correlation matrix, analysis of variance, and principal components analysis were  
198 conducted with SPSS version 18.0 (SPSS Inc., Chicago, IL, USA) to determine the possible  
199 relationships between the DOM parameters and environmental factors. A  $P$ -value  $\leq 0.05$  was  
200 considered significant. Regression analyses between the optical parameters of DOM and several  
201 biogeochemical parameters in the SSW and the SML samples were performed in the Table S1 and the  
202 Table S2, respectively.

### 203 3. Results and discussion

#### 204 3.1 Distribution and chemical characterization of DOM in the SSW of the eastern marginal seas of 205 China

206 The surface distributions of salinity, temperature, CDOM, DOC, Chl- $a$ , and several optical  
207 parameters in the study area during spring, summer and winter are shown in Fig. S3 (SSW)-S4 (SML)  
208 (Supporting Information). There was a strong south-to-north temperature gradient, with warmer waters  
209 in the ECS and cooler waters in the YS. Lower salinities were observed in the Changjiang Estuary and  
210 coastal waters. The lowest mean wind speed was observed in the summer of 2018 (Table 2). In spring  
211 and summer, the bacterial abundances were lower in the YS (spring mean concentration:  $2.26 \times 10^8$   
212 cells/L; summer mean concentration:  $3.79 \times 10^8$  cells/L) than in the ECS (spring mean:  $2.98 \times 10^8$   
213 cells/L; summer mean:  $7.64 \times 10^8$  cells/L), indicating that the warmer southern ECS had stronger  
214 biological activity in the SSW.

215 The  $a(254)$  value ranged from 1.08 to 19.28  $\text{m}^{-1}$  in the SML and from 0.82 to 14.23  $\text{m}^{-1}$  in the  
216 SSW during these three seasons. CDOM absorption values and DOC concentrations were generally  
217 decreased from the inshore to the offshore stations (Fig. S3 c-d)). Higher  $a(254)$  values were



218 generally observed in the Changjiang Estuary (spring: station D1 ( $4.13 \text{ m}^{-1}$ ); summer: station D2 ( $3.98$   
219  $\text{m}^{-1}$ ); winter: station D1 ( $3.14 \text{ m}^{-1}$ )) and in the northern YS (spring: station A2 ( $4.26 \text{ m}^{-1}$ ); summer:  
220 station H11 ( $5.37 \text{ m}^{-1}$ ); winter: station H12 ( $5.95 \text{ m}^{-1}$ )). There were significantly negative linear  
221 correlations between salinity and  $a(254)$  in all cruises in the SSW ( $p < 0.01$ , Fig. 2), especially in the  
222 ECS, implying that freshwater run-off and seawater mixing played a more important role in  
223 determining CDOM distributions in the SSW. The strongest negative linear relationship observed  
224 between salinity and  $a(254)$  was observed in winter when the influence of terrestrial input in this study  
225 region was maximal. In addition,  $SUVA_{254}$  ranged from 0.51 to  $8.39 \text{ L mg C}^{-1} \text{ m}^{-1}$  in the SML. In  
226 comparison with the SML, the SSW exhibited lower variability in  $SUVA_{254}$  values from 0.63 to  $5.39 \text{ L}$   
227  $\text{mg C}^{-1} \text{ m}^{-1}$ , with higher values at the northern YS stations and Changjiang Estuary coastal stations (Fig.  
228 S3k)). According to the  $SUVA_{254}$  trends observed by Massicotte et al. (2017), the DOM composition  
229 we observed in the SSW of the Changjiang Estuary ecosystem were more similar to the DOM  
230 measured in freshwater ecosystems than in the ocean.  $SUVA_{254}$  underwent a sharp decrease from the  
231 Changjiang Estuary ecosystem to the southeastern ECS, suggesting that aromatic and/or highly  
232 conjugated DOM moieties were degraded along the aquatic continuum from the Changjiang Estuary to  
233 the open ocean. Higher  $S_{275-295}$  values were also observed in some off-shore stations (Fig. S4i)). These  
234 comparisons showed that the DOM pools of the Changjiang Estuary contained molecules that were  
235 more HMW-DOM and contained more aromatic compounds, CDOM in the SSW of the southeastern  
236 ECS, which was derived predominantly from an autochthonous origin (phytoplankton production and  
237 bacterial activity), clearly showed the presence of organic matter freshly released into sea (Yang et al.,  
238 2020). The detail of mixing behavior, biological and photolytic degradation of dissolved organic  
239 matter in the East China Sea and the Yellow Sea were discussed in our previous paper (Yang et al.,



240 2020).

241

242 *3.2 Fluorescence signature and factors controlling the composition of FDOM components in the SSW*

243 *and the SML*

244 FDOM properties can be used as the sensitive indicator of DOM processing and water mass. Four  
245 fluorescent components were identified by PARAFAC analysis with the DOM Fluor toolbox in  
246 MATLAB 7.5 (Stedmon and Bro, 2008), hereafter named C1, C2, C3, and C4 (Fig. S2). The  
247 humic-like C1 and C3 were categorized as two traditional types of humic-like fluorescent components  
248 (Coble 1996). Component 1 had primary fluorescence excitation and emission peaks at 345 nm and  
249 455 nm, respectively, which was similar to terrestrial humic-like fluorophores in the visible region  
250 (peak C) (Osburn et al., 2012). Relative to C1, the fluorescence of C3 was blue-shifted and had  
251 fluorescence peaks at 385 nm emission and 315 nm excitation. The microbial humic-like component  
252 had a relatively shorter emission peak wavelength compared to the terrestrial humic-like PARAFAC  
253 components previously identified in the open ocean (Catala et al., 2015). C2 exhibited Ex/Em maxima  
254 at 255 nm/310 (375) nm, which could be considered tyrosine-like fluorescence (Stedmon et al., 2003)  
255 and attributed to autochthonous and/or microbially consumed FDOM. C4 had an excitation range of  
256 280 nm with an emission peak at 335 nm, which corresponded to peak T of the amino-acid-like  
257 fluorescence of tryptophan, likely derived from in situ primary autochthonous substances and other  
258 fresh biological sources (Coble, 1996). The tryptophan-like C4 and the humic-like C1 and C3 in the  
259 SSW were all negatively correlated with salinity ( $P < 0.01$ , Table S1), but increased with the  
260 increasing DO level. These suggested that water mixing and microbial activity were important factors  
261 in determining geographical distributions of FDOM in the SSW (Breitburg, et al., 2018; Yamashita et



262 al., 2017; Galgani and Engel, 2016). Moreover, the geographical distribution of humic-like C1 and  
263 protein-like components were more similar to that of the Chl-a concentration in the SML (Fig. 3 a, b,  
264 d). Such relationships suggested that the production of protein-like and humic-like FDOM with  
265 phytoplankton production and decay in the SML.

266 FDOM enrichment in the SML of all stations ranged between 0.5 and 11 ( $n = 225$ ) and FDOM  
267 was more frequently enriched (C1: 89.6%; C2: 73.2%; C3: 91.8%; C4: 93.4% of all samples) than  
268 CDOM. The fluorescence intensity of the components in the SML samples decreased in the following  
269 order: tryptophan-like > tyrosine-like > terrestrial humic-like > marine humic-like; whereas those in  
270 the SSW samples decreased in the order: tyrosine-like > tryptophan-like > marine humic-like >  
271 terrestrial humic-like. The tryptophan-like component (C4) was mostly enriched in the SML samples  
272 with a median EF = 2.2 and a range from 0.2 and 8.0. The EF of C4 was clearly higher than other  
273 components in all seasons (Fig. 5b)), especially in summer, and the FDOM composition in the SML  
274 revealed a relatively higher proportion of autochthonous tryptophan-like FDOM than the SSW. It has  
275 also been broadly recognized that tryptophan-like C4 in the particulate fraction is related to recent  
276 primary production (Brym et al., 2014; Yamashita, 2014) and that phytoplankton excrete  
277 tryptophan-like fluorophores (Romare-Castillo et al., 2010). Together, as already emphasized  
278 previously, the variation observed for FDOM can be more related to that of Chl-a in the SML, these  
279 observations suggested that the DOM enriched in the SML was made up of a relatively higher  
280 proportion of marine autochthonous DOM than the SSW.

281

### 282 3.3 DOM and biogenic molecules accumulation in the SML

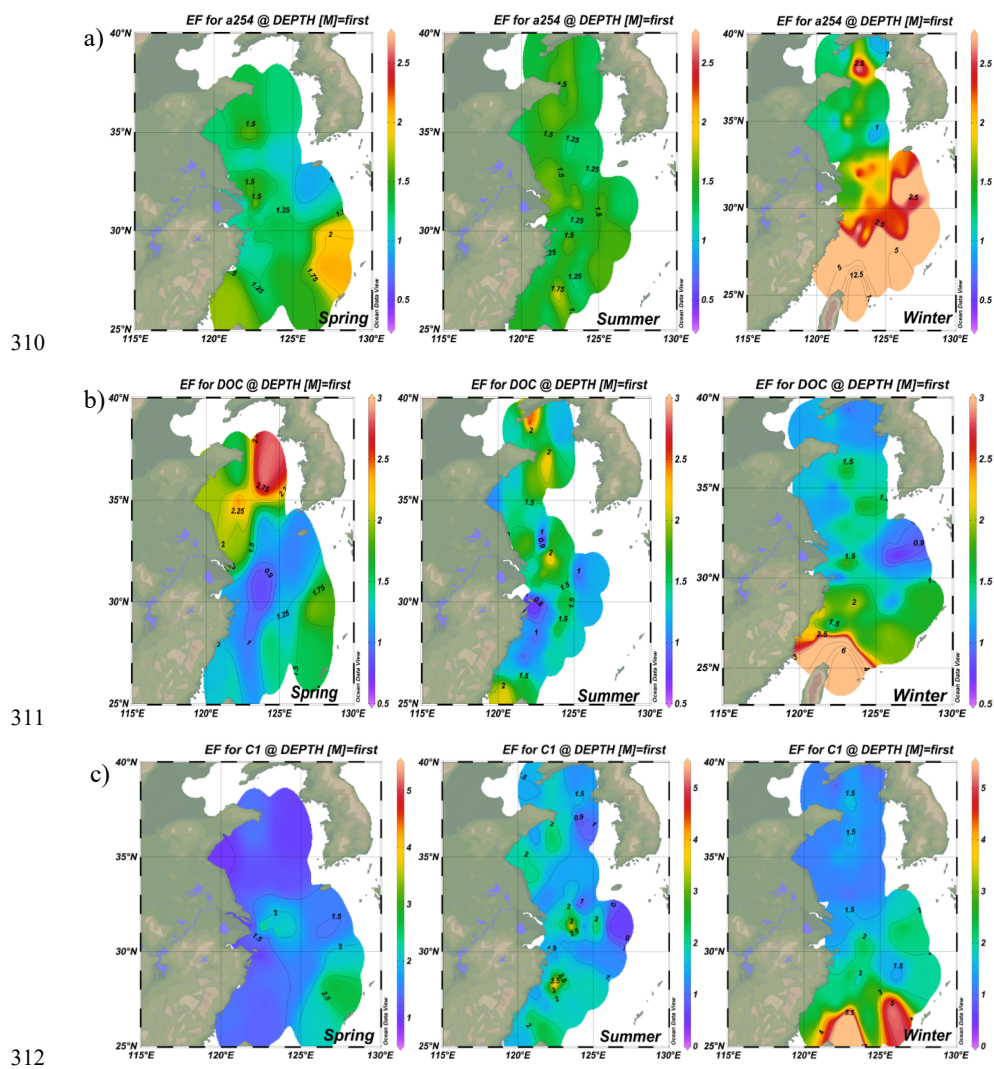
283 Up to 88% of our CDOM samples were enriched in the SML, with the median EF for a(254) of  
284 1.3, ranging between 0.4 and 6.7. Concentrations of CDOM, FDOM, nutrients, bacterial abundance,

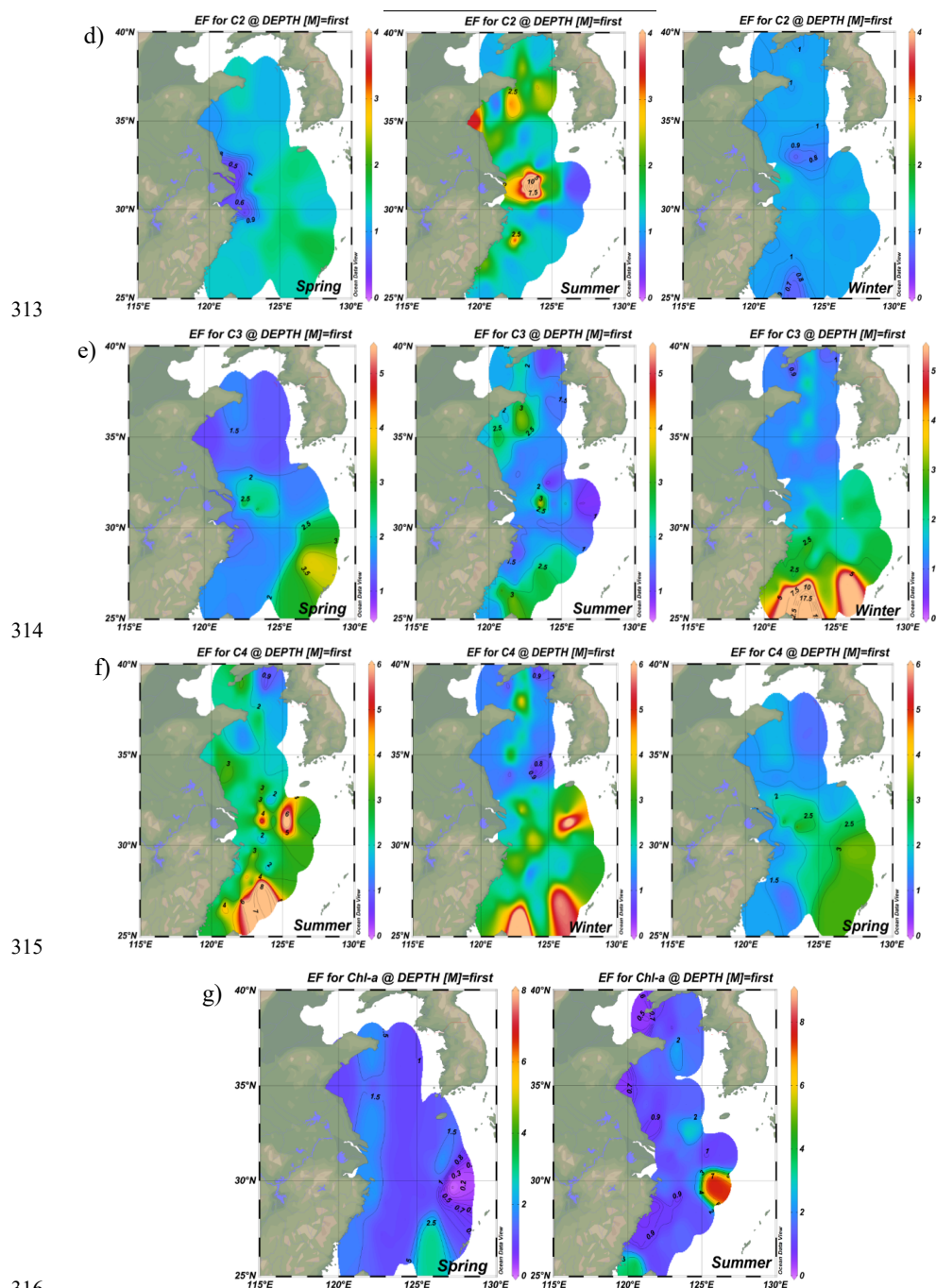


285 and Chl-*a* in the SML were correlated with their respective SSW concentrations (Fig. 4),  
286 demonstrating that transport from the SSW to the SML is an important pathway. Furthermore, the  
287 relatively higher CDOM absorption enrichment value in the SML were found at longer wavelengths  
288 (Fig. 5a))  $EF$  of  $a(355) > EF$  of  $a(254)$ ). Marine production of DOM had the largest influence on the  
289 CDOM absorption properties in the longer wavelength range (Danheiz et al., 2017) ( $S_{320-412}$ : DOM  
290 marine origin VS.  $S_{275-295}$ : terrestrial DOM). Galgani and Engel (2016) also observed that amino  
291 acid-like fluorophores were highly enriched in the SML, not only due to their amphiphilic properties,  
292 but also due to their local production in the SML. Therefore, the marine local production might  
293 significantly affect the composition of DOM in the SML. Additionally, the nutrients showed  
294 significantly higher  $EF$ s ( $NO_3^-$ :  $3.41 \pm 6.08$ ,  $n = 41$ ;  $NO_2^-$ :  $3.57 \pm 5.54$ ,  $n = 52$ ;  $PO_4^{3-}$ :  $2.13 \pm 2.74$ ,  $n =$   
295  $68$ ; and  $SiO_3^{2-}$ :  $6.53 \pm 13.67$ ,  $n = 13$ ) than biological and DOM parameters in the SML. The strong  
296 correlation between the SML and SSW concentrations of  $NO_2^-$ ,  $NO_3^-$ , and  $SiO_3^{2-}$  (Fig. 4) showed that  
297 the similar fundamental drivers are probably at work in both compartments for these nutrients. For  
298 example, dissolved substances, particles, and microorganisms were brought to the interface by simple  
299 diffusion, rising bubbles (Jarvis, 1967), convection, and upwelling from sediments and subsurface  
300 water, and at the same time, the microlayer is also a sink for fallout from the atmosphere (Duce et al.,  
301 1976). In addition, we also observed the significant positive relationship between  $a(254)$  and Chl-*a* ( $R$   
302  $= 0.662$ ,  $P < 0.01$ ) in the SML during spring, and the positive relationship between the  $EF$  of  $PO_4^{3-}$  and  
303 the  $EF$  of Chl-*a* ( $R = 0.319$ ,  $P = 0.01$ , Table 3). These observations indicated that spatial variation of  
304 CDOM concentrations were related to Chl-*a* in the SML. The enrichment of inorganic nutrients would  
305 be an important factor influencing the production and composition of phytoplankton-produced DOM  
306 (Carlson and Hansell, 2003) in the SML. Therefore, phytoplankton growth, primary productivity rate,



307 biological activity and marine autochthonous DOM production would all be enhanced by the enriched  
308 nutrients in the SML.  
309



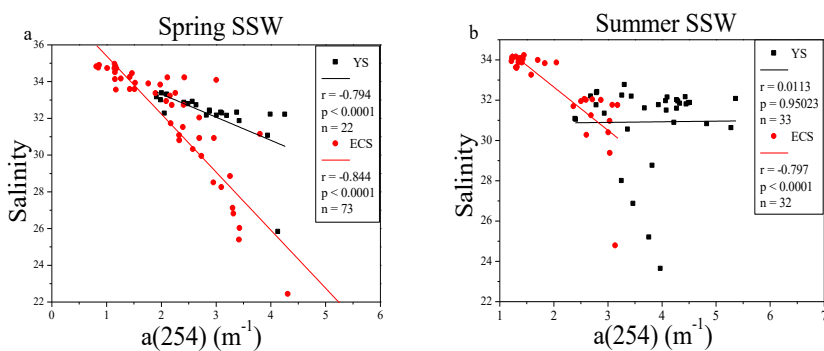


317 Fig. 1. Distributions of enrichment factors of CDOM, DOC, Chl-*a*, and four fluorescence components  
318 in the surface microlayer water during spring, summer, and winter. Increasing DOM yields were  
319 significant in coastal regions in all seasons, but the higher EFs were more pronounced in off-shore

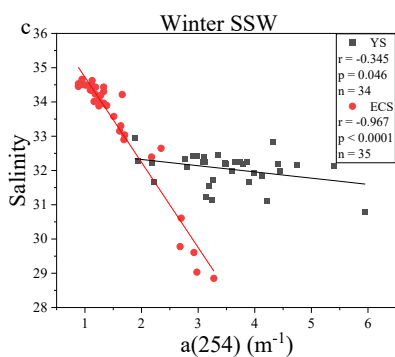


320

regions.



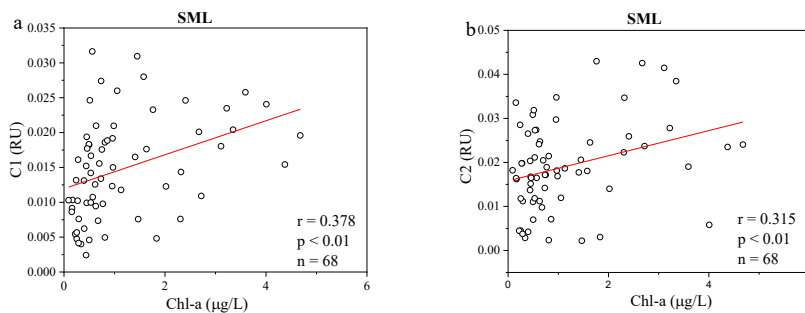
321



322

323 Fig. 2. Relationships between  $a(254)$  and salinity in the SSW in the YS and the ECS during spring,  
324 summer and winter.

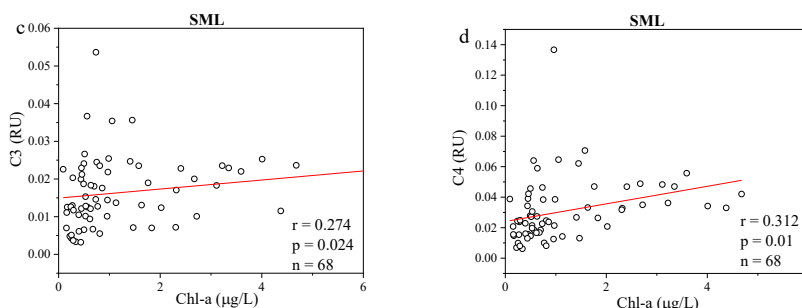
325



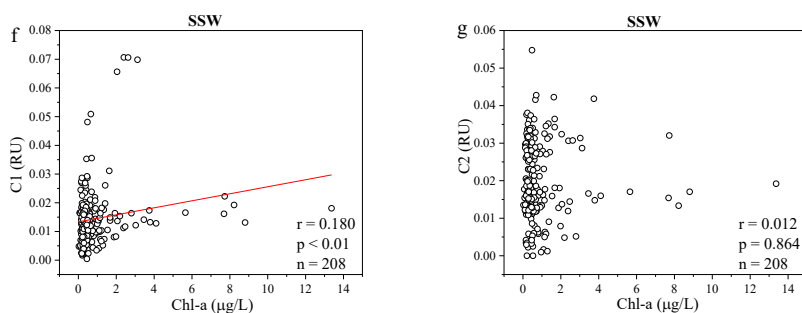
326



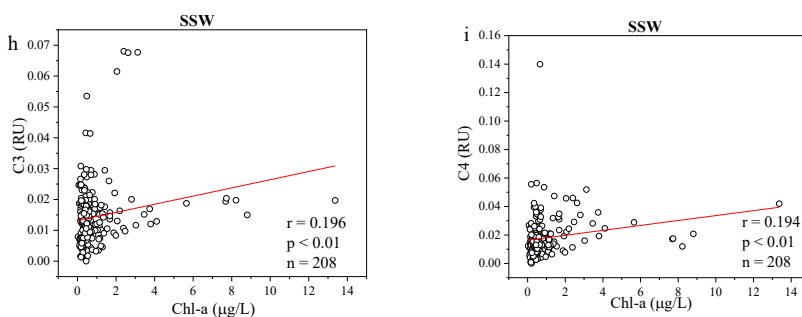
327



328



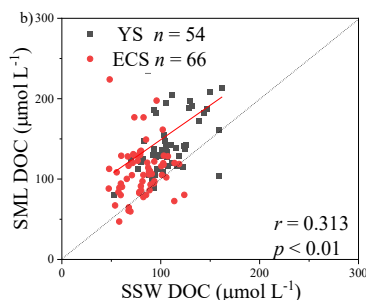
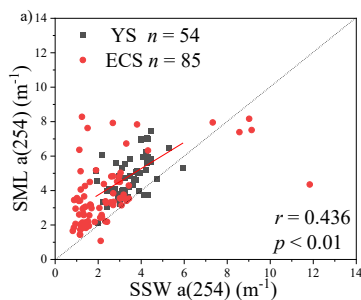
329



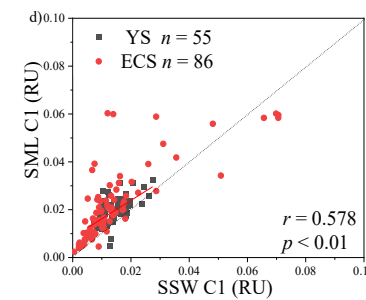
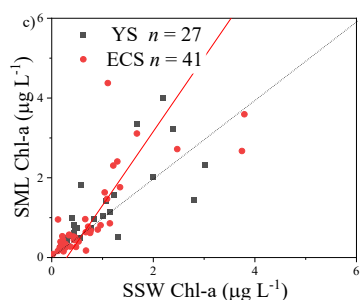
330 Fig. 3. Relationships between a(254), four fluorescence components and Chl-a in the SML (a-d) and in  
331 the SSW (f-i).



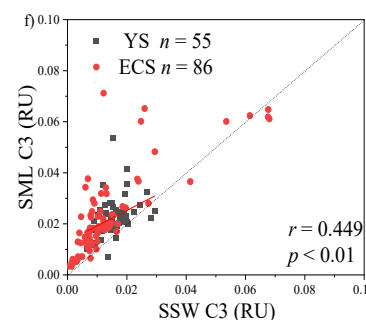
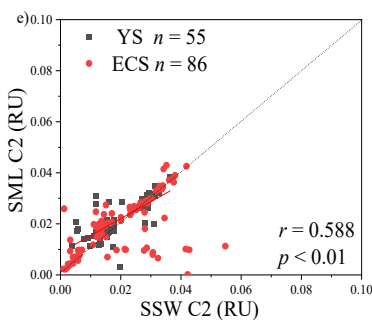
332



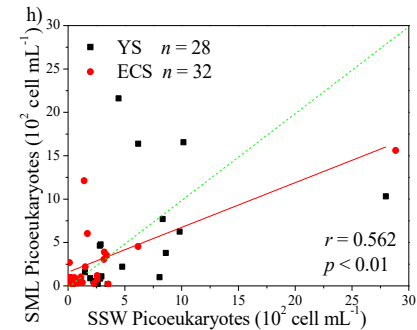
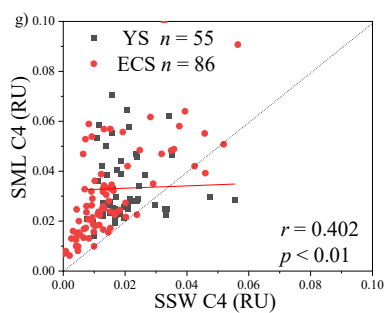
333



334



335



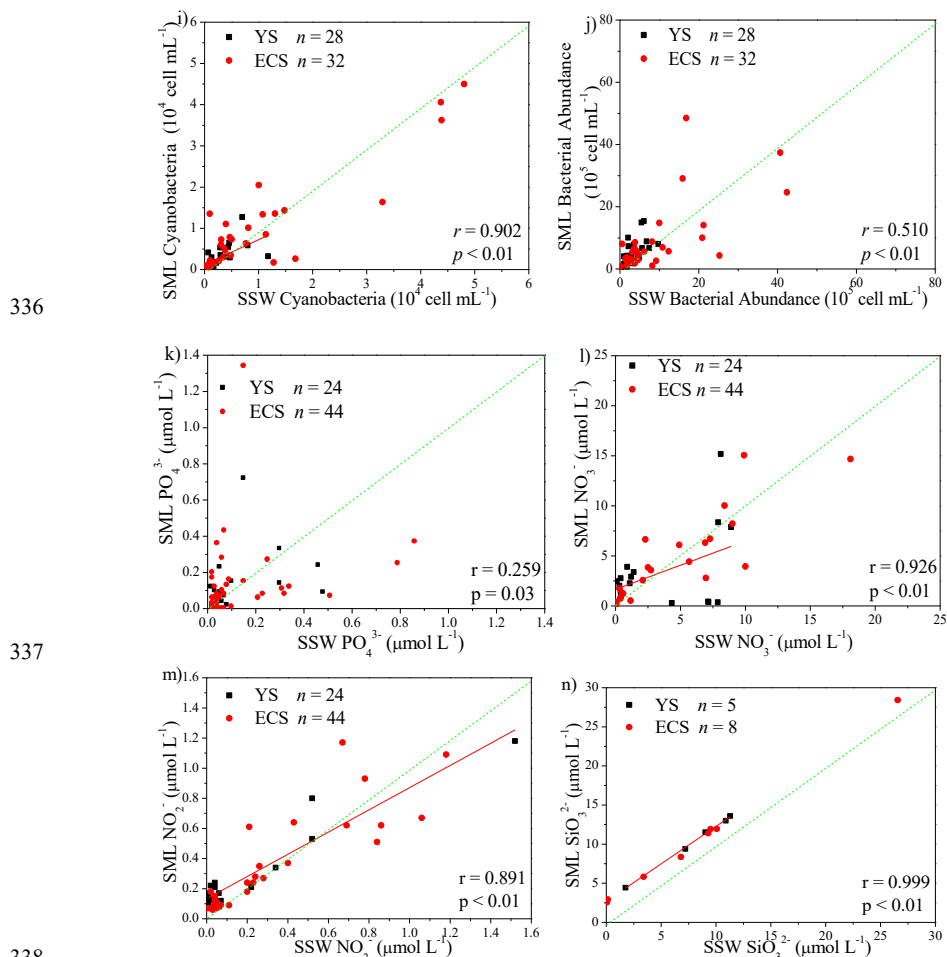
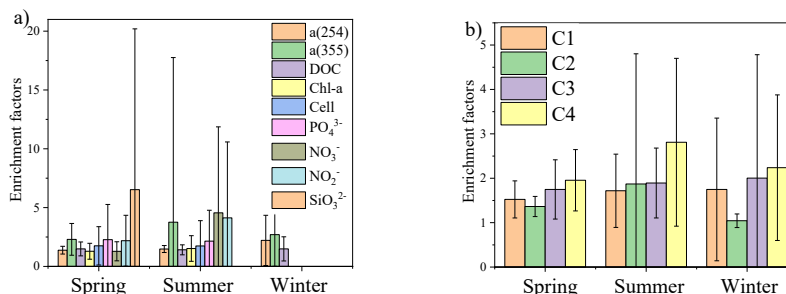


Fig. 4. Correlations between the microlayer CDOM, DOC, Chl-*a*, four fluorescence components concentrations, cyanobacteria, phytoplankton biomass, nutrients and bacterial abundance, and their subsurface water concentrations. The dashed lines correspond to the 1:1 lines, and the full lines are the regression models. (All DOM spectroscopic parameters sample were analyzed in spring, summer, autumn, and winter; Chl-*a* was determined in spring, summer, and summer; cyanobacteria, phytoplankton biomass, nutrients and bacterial abundance were determined in spring and summer.).



345

346 Fig. 5. Mean enrichment factor of  $a_{CDOM}$  (254 nm and 355 nm), DOC, Chl-*a*, nutrients ( $PO_4^{3-}$ ;  $NO_3^-$ ;  
347  $NO_2^-$ ,  $SiO_3^{2-}$ ), and four fluorescence components during spring, summer, and winter.

348

#### 349 3.4 Wind speed influencing the enrichment of DOM optical properties

350 The wind speeds during our observations ranged from 0.2 to 14.9 m s<sup>-1</sup>. We divided them into  
351 three different wind regimes: low (0.0–2.0 m s<sup>-1</sup>), moderate (2.0–10.0 m s<sup>-1</sup>), and high (10.0–14.9 m  
352 s<sup>-1</sup>). Although the EFs of DOC and Chl-*a* were negatively correlated with wind speed (DOC:  $P = 0.002$ ;  
353 Chl-*a*:  $P = 0.042$ ), the EFs of CDOM and FDOM were not. During the low wind regime, no  
354 significant relationships were apparent between wind speed and either EFs of CDOM or FDOM,  
355 CDOM and FDOM were consistently enriched, with EFs ranging from 1.0 to 2.2, and a mean  $a(254)$   
356 EF value of 1.3 ( $n = 20$ ). However, the EFs during moderate winds had larger variability and ranged  
357 from 0.9 to 14.5, with a mean EF value of 1.6 ( $n = 143$ ), and during high winds they ranged from 0.6  
358 to 1.8, with a lower mean EF value of 1.1 ( $n = 18$ ). In addition, depleted levels of CDOM (EF < 1)  
359 occurred at frequencies of 5.6%, 9.1%, and 20.0% during low, moderate, and high wind regimes,  
360 respectively. Therefore, although lower wind speeds and ascending bubbles might further promote the  
361 transportation of organic materials from the underlying waters, DOM enrichments were still observed  
362 at wind speeds up to > 10 m s<sup>-1</sup>. Reinthaler et al. (2008) also reported that higher enrichment was  
363 found at higher wind speeds. During moderate to high wind regimes, breaking waves not only can



364 disrupt the surface film and physically drive DOM back into the bulk water, but also facilitate the  
365 formation of the SML as rising bubble plumes transported DOM to the surface, resulting in wider  
366 ranges of EFs (Frew et al., 2004). Higher wind speed does enhance mixing (Reinthal et al., 2008),  
367 which can arguably favour transport of nutrients and DOM from the SSW equally (Wurl et al., 2011).  
368 Although wind speed appear to play an important role in the enrichment of surface-active DOM, the  
369 chemical composition of the SML influence its stability. For example, enrichments of sulphate  
370 half-ester groups in the SML (Wurl and Holmes, 2008) could increase stability because these groups  
371 can influence the intrinsic viscosity of marine polymers (Nichols et al., 2005) and sulphur-containing  
372 algal carbohydrates are less soluble and hydrolysable (Kok et al., 2000). Enrichment processes and  
373 biochemical processes of organic substances in the marine environment are all likely to be the more  
374 important contributors of DOM to the SML in our study regions.

### 375 *3.5 Photochemical degradation of DOM in the SSW and the SML*

376 Photobleaching is one of the major mechanisms determining the geographical distributions of  
377 chromophoric and fluorescent DOM in the ocean (Helms et al., 2008; Brinkmann et al., 2003; Siegel  
378 et al., 2005). The average SUVA<sub>254</sub> values in SSW were generally higher than those in the SML in our  
379 study regions (SSW:  $2.45 \pm 0.91 \text{ L mg}^{-1} \text{ m}^{-1}$  vs. SML:  $2.39 \pm 1.34 \text{ L mg}^{-1} \text{ m}^{-1}$ ), and the most  
380 obvious distinction happened in summer (Table 2). These indicated that although CDOM  
381 concentration in the SSW was lower than that in the SML, CDOM in the SSW has a higher degree of  
382 aromaticity compared to the SML. Thus we performed photochemical incubation experiments to  
383 confirm whether photochemical reactions influenced the differentiated aromaticity and photo-reactive  
384 features of DOM between the SML and the SSW.

385 After 88 h of exposure, the  $a(254)$  values were only 49.6%, 45.5%, 42.1%, 41.8% and 37.0% of

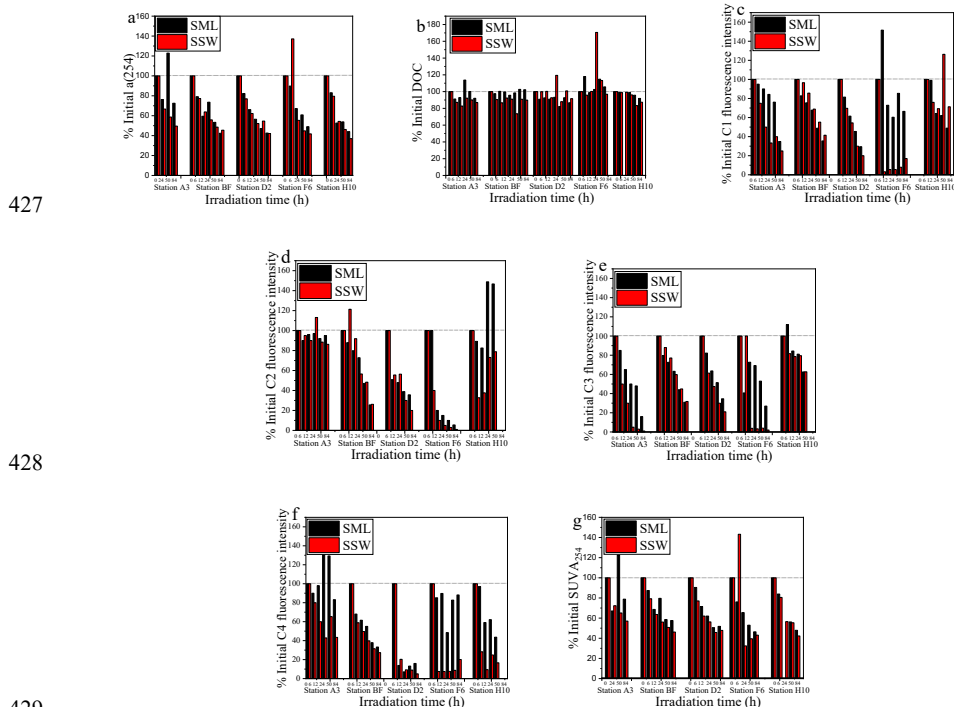


386 the initial values at stations A3, BF, D2, F6, and H10 in the SSW, and 72.5%, 42.4%, 42.6%, 49.0%  
387 and 44.0% of the initial values at stations A3, BF, D2, F6, and H10 in the SML, respectively. Overall,  
388  $a_{254}$  and  $SUVA_{254}$  decreased by  $49.9 \pm 12.8\%$  and  $43.0 \pm 15.5\%$ , respectively, in the SML, and by  
389  $56.8 \pm 4.7\%$  and  $56.0 \pm 10.2\%$ , respectively in the SSW. Therefore, stimulated solar UV exposure  
390 caused a larger decrease in DOM absorbance in the SSW than the SML (Fig. 6). The relatively rapid  
391 decrease of  $SUVA_{254}$  in the SSW indicated a more rapid conversion of DOM to less humic-type  
392 materials than in the SML. Approximately 65% of FDOM was lost during the irradiation experiment,  
393 except in the case of the tyrosine-like component 2 from the SML at the station H10, which increased  
394 slightly. Photoproduction of tyrosine-like components has been previously reported by Zhu et al.  
395 (2017), who suggested that the photochemical degradation of CDOM contributed to the release small  
396 amounts of tyrosine-like fluorophores. The tryptophan-like C4, humic-like C1 and C3 were more  
397 photodegraded in the SSW than in the SML (Fig. 6c, e, f). For example, C1, C3 and C4 show a  
398 marked decrease in the SSW at the off-shore station F6. Because of the origin of CDOM at the station  
399 F6 remote from the direct terrestrial influence, the majority of CDOM at the station F6 was thought to  
400 be a by-product of net primary production. The present results showed that a large fraction of the total  
401 CDOM in the SSW at the off-shore station F6 is still potentially sensitive to photooxidation. As  
402 already referred previously, CDOM in the SSW showed higher  $SUVA_{254}$  values, and higher  
403 percentages of humic-like DOM than in the SML. Therefore, the photochemically mediated shifts in  
404 DOM in the SSW were more pronounced than those in the SML in our incubation experiments, in  
405 terms of both absorption and fluorescence values.

406 This heterogeneity in the EFs and photochemical reactivities of FDOM components can be  
407 related to the chemical and structural nature, such as molecular weight, aromaticity or humification of



408 FDOM enrichment processes. Hydrophilic, carboxylic acid-bearing DOM moieties are preferentially  
409 degraded by simulated sunlight (Brinkmann et al., 2003). The largest fractions of photolabile DOM are  
410 made up of aromatic carbon rings or high double bond equivalent molecules (Kujawinski et al., 2004;  
411 Gonsior et al., 2009). The humic-like C1 and C3, all of which exhibited significantly positive  
412 relationships with  $SUVA_{254}$  ( $< 0.001$ , Table 1) and shown higher aromaticity, were more prone to  
413 photochemical degradation (Fig. 6c), e), and f)). The tyrosine-like C2, as compared to other  
414 protein-like compounds, is generally considered more labile and susceptible to bacterial cycling and  
415 rapid consumption by microbiota (Medeiros et al., 2015). The SML experiences the most intense solar  
416 radiation, especially ultraviolet (UV) light (Obenosterer et al., 2005). Photochemical degradation may,  
417 therefore, be a sink for aromaticity fluorescent components in the SML, and be a source for the  
418 tyrosine-like C2. In addition, Blough (1997) discovered that photochemical production rates in the  
419 SML should lead to the more rapid oxidative turnover of materials at the interface and potentially to  
420 reactions and processes not observed in bulk waters. Therefore, differences in  $SUVA_{254}$  values and  
421 photoreaction behavior between the SSW and the SML may also reflect that DOM in the SML was  
422 already photobleached, which resulted in the decrease of DOM aromaticity, CDOM in the SSW  
423 appeared to be more susceptible to photochemical degradation than CDOM in the SML. Together,  
424 photo-irradiation have the significant influence on the accumulation of protein-like DOM and  
425 depletion of aromatic organic compounds in the SML, and organic carbon might have undergone a  
426 more rapid cycling in the SML than the SSW.



427

428

429

430

431

432

Fig. 6. Changes in ratios of  $a(254)$ , DOC,  $SUVA_{254}$  and four fluorescence components intensities to initial values for both SML and SSW sample.

433

### 3.6 Variations in the enrichment factors of CDOM, DOC, FDOM along the coastal regions to ocean

434

The concentrations of  $a(254)$  and DOC decreased from the coastal regions to the open ocean, and

435

decreased from the northern part of the sampling area (the YS) to the southern part of the sampling

436

area (the ECS) in both the SSW and the SML (Fig. S3 c-d) and Fig. S4 a-b)). However, CDOM and

437

FDOM were more frequently enriched in the ECS (CDOM: 93% of all samples; FDOM: 72–94% of

438

all samples) than that in the YS (CDOM: 86% of all samples; FDOM: 70–92% of all samples). The

439

higher EF values for CDOM, FDOM, DOC, Chl-*a*, nutrients, and cell were generally observed in the

440

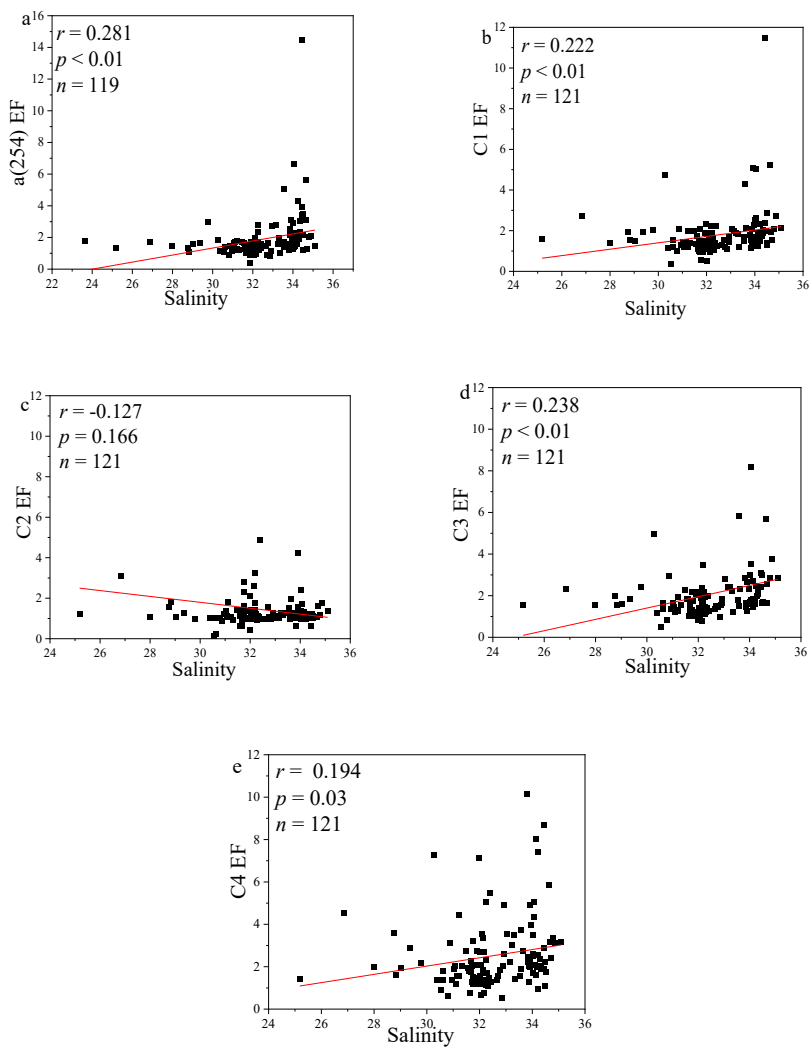
ECS (Fig. 1). Lower EFs and EFs < 1, which indicate a depletion of CDOM in the SML, were usually

441

observed at short distances from the coast (Fig. 1) with lower salinity. The salinity during our



442 observations ranged from 23.6 to 35.1. Although CDOM and FDOM concentration negatively  
443 correlated with salinity, the EFs of CDOM and FDOM were weakly positive related with salinity (Fig.  
444 7). The EFs of Chl-*a* and nutrient were also higher in the southeastern ECS (Fig. 1 and Fig. S5), where  
445 sufficient light and higher temperature combined to facilitate primary production and higher  
446 contributions of autochthonous materials to DOM. DOM in the SSW of the southern ECS was more  
447 dominated by marine autochthonous materials in our previous discussion (Yang et al., 2020). The  
448 Changjiang River discharges enormous amounts of N and P into the ECS (Liu et al., 2018), but  
449 phosphorus is generally the major limiting element for phytoplankton growth in the ECS (Liu et al.,  
450 2016). Thus the difference in EFs of CDOM and Chl-*a* between YS and the ECS, and between the  
451 coast and off-shore regions is likely due to the significantly nutrients enrichment in the SML in the  
452 off-shore regions. In winter, we observed especially higher EF values for CDOM and FDOM in the  
453 southern ECS (Fig. 1a-f)). With wind from the northwest (Weng et al., 2011), biologically essential  
454 trace elements and anthropogenic emissions are carried from the land and can enter the ocean via the  
455 SML by wet or dry deposition. The EFs of humic-like C1 and C3 were relatively high in winter (Fig.  
456 5b)), probably due to the input from atmospheric deposition during winter, and the relatively low  
457 CDOM concentrations in bulk water. Atmospheric deposition of organic carbon and nutrients were  
458 found a peak in winter over the coastal ECS (Wang et al., 2019). We suggested that the EFs of CDOM  
459 and FDOM increased from the coastal regions to the open ocean, and increased from the YS to the  
460 ECS were likely due to the enrichment of enough nutrients in the SML in the open ocean promote  
461 phytoplankton biomass and DOM production.



462

463

464

465

466

Fig. 7. Relationships between salinity and EFs of  $a(254)$ , Chl-a, DOC, and four fluorescence components.



467       The SML is an aggregate-enriched biofilm environment with distinct microbial communities,  
468       where the diversity of microorganisms can differ significantly from those of underlying waters (Liss  
469       and Duce, 2005; Cunliffe et al., 2013), the heterotrophic bacterial abundance in the SML was ~ 7.5  
470       fold greater than those in the SSW in the ECS during our spring cruise (Sun et al., 2020). Here, EFs  
471       showed a greater presence of bacteria and marine protein-like DOM in the SML than that in the SSW,  
472       while the protein-like DOM was linked to microbial utilization and degraded faster than the humic-like  
473       substances (Yang et al., 2017; Jørgensen et al., 2011). Therefore, compared to coastal waters that have  
474       larger terrestrial DOM and nutrients inputs, CDOM shown higher EFs in off-shore regions where  
475       DOM in the SSW is mostly of marine autochthonous origin with higher temperatures and stronger  
476       biological activity. The significantly higher abundance of cells, phytoplankton, nutrients, and  
477       protein-like DOM in the SML supported microbial activities, and further contributing to the local  
478       release of marine extracellular DOM directly from microbes in the SML in the off-shore regions.  
479       When exposed to higher light intensities (summer), obviously enhance mineralization of DOM in the  
480       SML, and relatively less photochemical degradation in SSW could result in lower percentage of  
481       aromatic DOM in SML than the SSW. We concluded that SML CDOM dynamics can be expressed as  
482       a simple balance among enrichment process, primary production and photochemical destruction. Thus,  
483       higher EF of DOM in the SML in off-shore regions are likely supported by a favorable combination of:  
484       1) deposition and accumulation of amphiphilic compounds, 2) importance of bubble for upward  
485       transport of DOM and enrichment in SML, and 3) new production of DOM within the SML as a  
486       consequence of higher nutrients enrichment and the primary production.

487

#### 488   **4. Conclusions**



489 This study has provided the first data set that considers the distributions of CDOM, FDOM, DOC,  
490 Chl-*a*, nutrients, and bacterial abundances in the SML and SSW of the ECS and the YS during spring,  
491 summer, and winter. We have observed that the CDOM distribution related variability in primary  
492 production in the SML. Furthermore, we have demonstrated that localized and stronger photochemical  
493 oxidation may be responsible for the decrease in the aromaticity of the DOM in the SML, due to  
494 enhanced transformation or removal of terrestrial DOM, compared with the SSW. We also  
495 demonstrated that in off-shore seawaters away from terrigenous influence, the EFs of CDOM, DOC,  
496 FDOM and Chl-*a* in SML tend to be higher in off-shore regions than those in coastal regions, because  
497 of the relatively higher enrichment of nutrients which could enhance phytoplankton growth and  
498 promoted plant production and DOM production in the SML. Multiple observations of spatial  
499 distributions, seasonal variations, chemical compositions, and photochemical reactions of CDOM in  
500 the SML have supported the hypothesis that stronger enrichment and photochemical processes occur in  
501 the SML in ocean, resulting in relatively accelerated enrichment of more marine local production  
502 DOM in the SML than the SSW.

503

#### 504 **Acknowledgements**

505 We thank the captain and crews of the R/V ‘*Dong Fang Hong 2*’, the R/V ‘*Dong Fang Hong 3*’,  
506 and the R/V ‘*Zhe Yu 2*’ for their assistance and cooperation during the investigation. We gratefully  
507 acknowledge Ya-Hui Gao (Xiamen University), Yu Xin (Ocean University of China), and Xiao-Hua  
508 Zhang (Ocean University of China) for providing the Chl-*a*, nutrients, bacterial abundance and  
509 picoplankton data, respectively. This work was financially supported by the National Key Research  
510 and Development Program (Grant No. 2016YFA0601304), and the National Natural Science  
511 Foundation of China (Grant Nos. 41806093 and 491830534).

512



513

## References

514 Aller, J.Y., Kuznetsova, M., Jahns, C.J., Kemp, P.F., 2005. The sea surface microlayer as a source of  
515 viral and bacterial enrichment in marine aerosols. *J. Aerosol Sci.* 36(5), 801–812.  
516 <https://doi.org/10.1016/j.jaerosci.2004.10.012>

517 Breitburg, D., Levin, L.A., Oschlies, A., Grégoire, M., Chavez, F.P., Conley, D.J., Garçon, V., Gilbert,  
518 D., Gutiérrez, D., Isensee, K., Jacinto, G.S., Limburg, K.E., Montes, I., Naqvi, S.W.A., Pitcher,  
519 G.C., Rabalais, N.N., Roman, M.R., Rose, K.A., Seibel, B.A., Telszewski, M., Yasuhara, M.,  
520 Zhang, J., Declining oxygen in the global ocean and coastal waters. *Science* 2018, 5, 359(6371),  
521 eaam7240. <https://doi.org/10.1126/science.aam7240>

522 Brinkmann, T., Sartorius, D., Frimmel, F.H., 2003. Photobleaching of humic rich dissolved organic  
523 matter. *Aquat. Sci.* 65(4), 415–424.

524 Brym, A., Paerl, H.W., Montgomery, M.T., Handsel, L.T., Ziervogel, K., Osburn, C.L., 2014. Optical  
525 and chemical characterization of base-extracted particulate organic matter in coastal marine  
526 environments. *Mar. Chem.* 162(6), 96–113. <https://doi.org/10.1007/s00027-003-0670-9>

527 Carlson, C.A., Hansell, D.A., 2003. The contribution of dissolved organic carbon and nitrogen to  
528 biogeochemistry of the Ross Sea. In: DiTullio, G., Dunbar, R. (Eds.), *Biogeochemical Cycles in  
529 the Ross Sea*. AGU Press, Washington DC, pp. 123–142.

530 Carpenter, J.H., 1964. The Chesapeake Bay Institute technique for the Winkler dissolved oxygen  
531 method. *Limnol. Oceanogr.* 10(1964), 141–143. <https://doi.org/10.4319/lo.1965.10.1.0141>

532 Catala, T.S., Reche, I., Fuenteslema, A., Romeracastillo, C., Nietocid, M., Ortegaretuerta, E.,  
533 Alvarezsalgado, X.A., 2015. Turnover time of fluorescent dissolved organic matter in the dark



- 534 global ocean. *Nat. Com.* 6(1), 5986–5993. <https://doi.org/10.1038/ncomms6986>
- 535 Chen, Y., Yang, G., Xia, Q., Wu, G., 2016. Enrichment and characterization of dissolved organic  
536 matter in the surface microlayer and subsurface water of the South Yellow Sea. *Mar. Chem.*  
537 182(Mar. 20), 1–13. <https://doi.org/10.1016/j.marchem.2016.04.001>
- 538 Chowdhury, S., 2013. Trihalomethanes in drinking water: Effect of natural organic matter distribution.  
539 *Water SA* 39(1), 1–7. <https://doi.org/10.4314/wsa.v39i1.1>
- 540 Coble, P.G., 1996. Characterization of marine and terrestrial DOM in seawater using  
541 excitation-emission matrix spectroscopy. *Mar. Chem.* 51(4), 325–346.  
542 [https://doi.org/10.1016/0304-4203\(95\)00062-3](https://doi.org/10.1016/0304-4203(95)00062-3)
- 543 Coble, P.G., 2007. Marine optical biogeochemistry: the chemistry of ocean color. *Chem. Rev.* 107(2),  
544 402–418. <https://doi.org/10.1002/chin.200720265>
- 545 Cunliffe, M., Engel, A., Frka, S., Gasparovic, B., Guitart, C., Murrell, J.C., Wurl, O., 2013. Sea surface  
546 microlayers: A unified physicochemical and biological perspective of the air–ocean interface.  
547 *Prog. Oceanogr.* 109(Feb.), 104–116. <https://doi.org/10.1016/j.pocean.2012.08.004>
- 548 Danhiez, F.P., Vantrepotte, V., Cauvin, A., Lebourg, E., Loisel, H., 2017. Optical properties of  
549 chromophoric dissolved organic matter during a phytoplankton bloom. Implication for DOC  
550 estimates from CDOM absorption. *Limnol. Oceanogr.* 62(4), 1409–1425.  
551 <https://doi.org/10.1002/lno.10507>
- 552 Duce, R.A., Hoffman, G.L., Ray, B.J., Fletcher, I.S., Wallace, G.T., Fasching, J.L., Piotrowicz, S.R.,  
553 Walsh, P.R., Hoffman, E.J., Miller, J.M., Heffter, J.L., 1976. Trace metals in the marine  
554 atmosphere: Sources and fluxes, in: *Marine Pollutant Transfer* (H. L. Windom and R. A. Duce,  
555 eds.), pp. 77–119, Lexington Books, Lexington.
- 556 Engel, A., Galgani, L., 2016. The organic sea-surface microlayer in the upwelling region off the coast



- 557 of Peru and potential implications for air–sea exchange processes. *Biogeosciences* 13(4),  
558 989–1007. <https://doi.org/10.5194/bg-13-989-2016>
- 559 Frew, N.M., Bock, E.J., Schimpf, U., Hara, T., Hausecker, H., Edson, J.B., Jahne, B., 2004. Air-sea gas  
560 transfer: Its dependence on wind stress, small-scale roughness, and surface films. *J. Geophys.*  
561 *Res.-Oceans* 109(C8), S17. <https://doi.org/10.1029/2003JC002131>
- 562 Galgani, L., Engel, A., 2016. Changes in optical characteristics of surface microlayers hint to  
563 photochemically and microbially mediated DOM turnover in the upwelling region off the coast of  
564 Peru. *Biogeosciences* 13(8), 2453–2473. <https://doi.org/10.5194/bg-13-2453-2016>
- 565 Garrett, W.D., 1965. Collection of slick-forming materials from the sea surface. *Limnol. Oceanogr.*  
566 10(1965), 602–605. <https://doi.org/10.2307/2833459>
- 567 Gonsior, M., Peake, B.M., Cooper, W.T., Podgorski, D., D’Andrilli, J., Cooper, W.J., 2009.  
568 Photochemically induced changes in dissolved organic matter identified by ultrahigh resolution  
569 fourier transform ion cyclotron resonance mass spectrometry. *Environ. Sci. Technol.* 43(3),  
570 698–703. <https://doi.org/10.1021/es8022804>
- 571 Grasshoff, K., Kremling, K., Ehrhardt, M., 2007. *Methods of Seawater Analysis*, 3rd. Edition. pp.  
572 407–420.
- 573 Guo, W., Yang, L., Zhai, W., Chen, W., Osburn, C.L., Huang, X., Li, Y., 2014. Runoff-mediated  
574 seasonal oscillation in the dynamics of dissolved organic matter in different branches of a large  
575 bifurcated estuary-The Changjiang Estuary. *J. Geophys. Res.-Biogeosciences* 119, 776–793.  
576 <https://doi.org/10.1002/2013JG002540>
- 577 Hardy, J.T., 1982. The sea surface microlayer: Biology, chemistry and anthropogenic enrichment. *Prog.*  
578 *Oceanogr.* 11(4), 307–328. [https://doi.org/10.1016/0079-6611\(82\)90001-5](https://doi.org/10.1016/0079-6611(82)90001-5)
- 579 Hardy, J.T., Apts, C.W., 1989. Photosynthetic carbon reduction: high rates in the sea-surface



- 580 microlayer. *Mar. Biol.* 101(3), 411–417. <https://doi.org/10.1007/BF00428138>
- 581 Helms, J.R., Stubbins, A., Ritchie, J.D., Minor, E.C., Kieber, D.J., Mopper, K., 2008. Absorption  
582 spectral slopes and slope ratios as indicators of molecular weight, source, and photobleaching of  
583 chromophoric dissolved organic matter. *Limnol. Oceanogr.* 53(3), 955–969.  
584 <https://doi.org/10.4319/lo.2008.53.3.0955>
- 585 Hoge, F.E., Vodacek, A., Blough, N.V., 1993. Inherent optical properties of the ocean: retrieval of the  
586 absorption coefficient of chromophoric dissolved organic matter from fluorescence measurements.  
587 *Limnol. Oceanogr.* 38(7), 1394–1402. <https://doi.org/10.4319/lo.1993.38.7.1394>
- 588 Jarvis, N.L., 1967. Adsorption of surface-active material at the sea-air interface, *Limnol. Oceanogr.* 12,  
589 213–221. <https://doi.org/10.4319/lo.1967.12.2.0213>
- 590 Jørgensen, L., Stedmon, C.A., Kragh, T., Markager, S., Middelboe, M., Søndergaard, M., 2011. Global  
591 trends in the fluorescence characteristics and distribution of marine dissolved organic matter. *Mar.*  
592 *Chem.* 126(1–4), 139–148. <https://doi.org/10.1016/j.marchem.2011.05.002>
- 593 Kieber, D.J., Mcdaniel, J., Mopper, K., 1989. Photochemical source of biological substrates in sea  
594 water: implications for carbon cycling. *Nature* 341(6243), 637–639.  
595 <https://doi.org/10.1038/341637a0>
- 596 Kok, M., Schouten, S., Sinninghe Damsté J.S., 2000. Formation of insoluble, nonhydrolyzable,  
597 sulfur-rich macromolecules via incorporation of inorganic sulfur species into algal carbohydrates.  
598 *Geochim. Cosmochim. Acta* 64(15), 2689–2699. [https://doi.org/10.1016/S0016-7037\(00\)00382-3](https://doi.org/10.1016/S0016-7037(00)00382-3)
- 599 Liss, P.S., Duce, R.A., 1997. *The Sea Surface and Global Change*, Cambridge University Press, 519.
- 600 Liss, P.S., Duce, R.A., 2005. *The Sea Surface and Global Change*. Cambridge University Press: UK.



- 601 Liu, S.M., Qi, X.H., Li, X.N., Ye, H.R., Wu, Y., Ren, J.L., Zhang, J., Xu, W.Y., 2016. Nutrient  
602 dynamics from the Changjiang (Yangtze River) estuary to the East China Sea. *J. Mar. Syst.*  
603 154(Feb.), 15–27. <https://doi.org/10.1016/j.jmarsys.2015.05.010>
- 604 Liu, X., Beusen, A.H.W., Van Beek, L.P.H., Mogollón, J.M., Ran, X., Bouwman, A.F., 2018. Exploring  
605 spatiotemporal changes of the Yangtze River (Changjiang) nitrogen and phosphorus sources,  
606 retention and export to the East China Sea and Yellow Sea. *Water Res.* 142(Oct. 1), 246–255.  
607 <https://doi.org/10.1016/j.watres.2018.06.006>
- 608 Margolin, A.R., Gonnelli, M., Hansell, D.A., Santinelli, C., 2018. Black sea dissolved organic matter  
609 dynamics: insights from optical analyses. *Limnol. Oceanogr.* 63(3), 1425–1443.  
610 <https://doi.org/10.1002/lno.10791>
- 611 Marie, D., Partensky, F., Jacquet, S., Vaulot, D., 1997. Enumeration and cell cycle analysis of natural  
612 populations of marine picoplankton by flow cytometry using the nucleic acid stain SYBR Green I.  
613 *Appl. Environ. Microbiol.* 63(1), 186–193. <https://doi.org/10.1109/50.337494>
- 614 Massicotte, P., Asmala, E., Stedmon, C., Markager, S., 2017. Global distribution of dissolved organic  
615 matter along the aquatic continuum: Across rivers, lakes and oceans. *Sci. Total Environ.* 609(Dec.  
616 31), 180–191. <https://doi.org/10.1016/j.scitotenv.2017.07.076>
- 617 Mcknight, D.M., Boyer, E.W., Westerhoff, P., Doran, P.T., Kulbe, T., Andersen, D.T., 2001.  
618 Spectrofluorometric characterization of dissolved organic matter for indication of precursor  
619 organic material and aromaticity. *Limnol. Oceanogr.* 46(1), 38–48.  
620 <https://doi.org/10.4319/lo.2001.46.1.0038>
- 621 Medeiros, P.M., Seidel, M., Ward, N.D., Carpenter, E.J., Gomes, H.R., Niggemann, J., Dittmar, T.,  
622 2015. Fate of the Amazon River dissolved organic matter in the tropical Atlantic Ocean. *Global*  
623 *Biogeochem. Cycl.* 29(5), 677–690. <https://doi.org/10.1002/2015GB005115>



- 624 Mopper, K., Kieber, D.J., 2002. Photochemistry and the cycling of carbon, sulfur, nitrogen and  
625 phosphorus. In: Hansell DA, Carlson CA (eds) Biogeochemistry of dissolved organic matter.  
626 Academic Press, San Diego, pp. 455–507.
- 627 Momzikoff, A., Brinis, A., Dallot, S., Gondry, G., Saliot, A., Lebaron, P., 2004. Field study of the  
628 chemical characterization of the upper ocean surface using various samplers. *Limnol. Oceanogr.*  
629 *Methods* 2(11), 374–384. <https://doi.org/10.4319/lom.2004.2.374>
- 630 Nichols, C.M., Lardière, S.G., Bowman, J.P., Nichols, P.D., Gibson, J.A.E., Guézennec, J., 2005.  
631 Chemical Characterization of Exopolysaccharides from Antarctic Marine Bacteria. *Microb. Ecol.*  
632 49(4), 578–589. <https://doi.org/10.1007/s00248-004-0093-8>
- 633 Obernosterer, I., Catala, P., Reinthaler, T., Herndl, G.J., Lebaron, P., 2005. Enhanced heterotrophic  
634 activity in the surface microlayer of the Mediterranean Sea. *Aquat. Microb. Ecol.* 39(3), 293–302.  
635 <https://doi.org/10.3354/ame039293>
- 636 Ogawa, H., Amagai, Y., Koike, I., Kaiser, K., Benner, R., 2001. Production of refractory dissolved  
637 organic matter by bacteria. *Science* 292(5518), 917–920.  
638 <https://doi.org/10.1126/science.1057627>
- 639 Orellana, M.V., Matrai, P.A., Leck, C., Rauschenberg, C.D., Lee, A.M., Coz, E., 2011. Marine  
640 microgels as a source of cloud condensation nuclei in the high Arctic. *Proc. Natl. Acad. Sci.*  
641 108(33), 13612–13617. <https://doi.org/10.1073/pnas.1102457108>
- 642 Ortega-Retuerta, E., Passow, U., Duarte, C.M., Reche, I., 2009. Effects of ultraviolet B radiation on  
643 (not so) transparent exopolymer particles. *Biogeosciences* 6(12), 3071–3080.  
644 <https://doi.org/10.5194/bg-6-3071-2009>
- 645 Osburn, C.L., Handsel, L.T., Mikan, M.P., Paerl, H.W., Montgomery, M.T., 2012. Fluorescence



- 646 tracking of dissolved and particulate organic matter quality in a river-dominated estuary. Environ.  
647 Sci. Technol. 46(16), 8628–8636. <https://doi.org/10.1021/es3007723>
- 648 Parsons, T.R., Matia, Y., Lalli, C.M., 1984. A Manual of Chemical and Biological Methods for  
649 Seawater Analysis. Pergamon Press, Oxford.
- 650 Reinthaler, T., Sintes, E., Herndl, G.J., 2008. Dissolved organic matter and bacterial production and  
651 respiration in the sea-surface microlayer of the open Atlantic and the western Mediterranean sea.  
652 Limnol. Oceanogr. 53(1), 122–136. <https://doi.org/10.4319/lo.2008.53.1.0122>
- 653 Romera-castillo, C., Sarmiento, H., Alvarezsalgado, X.A., Gasol, J.M., Marrase, C., 2010. Production  
654 of chromophoric dissolved organic matter by marine phytoplankton. Limnol. Oceanogr. 55(1),  
655 446–454. <https://doi.org/10.4319/lo.2010.55.1.0446>
- 656 Siegel, D.A., 2005. Colored dissolved organic matter and its influence on the satellite - based  
657 characterization of the ocean biosphere. Geophys. Res. Lett. 32(20), 469–496.  
658 <https://doi.org/10.1029/2005GL024310>
- 659 Singh, S., D'Sa, E., Swenson, E., 2010. Seasonal variability in CDOM absorption and fluorescence  
660 properties in the Barataria Basin, Louisiana, USA. J. Environ. Sci. 22(10), 1481–1490.  
661 [https://doi.org/10.1016/S1001-0742\(09\)60279-5](https://doi.org/10.1016/S1001-0742(09)60279-5)
- 662 State Bureau of Technical Supervision Bureau, 1992. Specifications for Oceanographic Survey-Survey  
663 of Biology in Sea Water. Standard Press of China, Beijing, pp. 17–20.
- 664 Stedmon, C.A., Bro, R., 2008. Characterizing dissolved organic matter fluorescence with parallel  
665 factor analysis: a tutorial. Limnol. Oceanogr.-methods 6(11), 572–579.  
666 <https://doi.org/10.4319/lom.2008.6.572b>
- 667 Stedmon, C.A., Markager, S., 2005. Resolving the variability in dissolved organic matter fluorescence  
668 in a temperate estuary and its catchment using PARAFAC analysis. Limnol. Oceanogr. 50(2),  
669 686–697. <https://doi.org/10.4319/lo.2005.50.2.0686>



- 670 Stedmon, C.A., Markager, S., Bro, R., 2003. Tracing dissolved organic matter in aquatic environments  
671 using a new approach to fluorescence spectroscopy. *Mar. Chem.* 82(3–4), 239–254.  
672 [https://doi.org/10.1016/s0304-4203\(03\)00072-0](https://doi.org/10.1016/s0304-4203(03)00072-0)
- 673 Stedmon, C.A., Markager, S., Tranvik, L., Kronberg, L., Slätis, T., Martinsen, W., 2007.  
674 Photochemical production of ammonium and transformation of dissolved organic matter in the  
675 Baltic Sea. *Mar. Chem.* 104(3–4), 227–240. <https://doi.org/10.1016/j.marchem.2006.11.005>
- 676 Su, Y., Hu, E., Feng, M., Zhang, Y., Chen, F., Liu, Z., 2017. Comparison of bacterial growth in  
677 response to photodegraded terrestrial chromophoric dissolved organic matter in two lakes. *Sci.*  
678 *Total. Environ.* 579(Feb. 1), 1203–1214. <https://doi.org/10.1016/j.scitotenv.2016.11.104>
- 679 Sun, H., Zhang, Y.H., Tan, S., Zheng, Y.F., Zhou, S., Ma, Q.Y., Yang, G.P., Todd, J., Zhang, X.H., 2020.  
680 DMSP-Producing Bacteria Are More Abundant in the Surface Microlayer than Subsurface  
681 Seawater of the East China Sea. *Microb. Ecol.* 80(1), 350–365.  
682 <https://doi.org/10.1007/s00248-020-01507-8>
- 683 Wang, F., Feng, T., Guo, Z., Li, Y., Lin, T., Rose, N.L., 2019. Sources and dry deposition of  
684 carbonaceous aerosols over the coastal East China Sea: Implications for anthropogenic pollutant  
685 pathways and deposition. *Environ. Pollut.* 245(Feb.), 771–779.  
686 <https://doi.org/10.1016/j.envpol.2018.11.059>
- 687 Weishaar, J.L., Aiken, G.R., Bergamaschi, B.A., Fram, M.S., Fujii, R., Mopper, K., 2003. Evaluation  
688 of specific ultraviolet absorbance as an indicator of the chemical composition and reactivity of  
689 dissolved organic carbon. *Environ. Sci. Technol.* 37(20), 4702–4708.  
690 <https://doi.org/10.1021/es030360x>
- 691 Weng, H., Tian, R., Ji, Z., Yu, X., 2011. Potential relationships between atmospheric particulate matter



- 692 transported by winter monsoons and red tides in the East China Sea. *Sci. Bull.* 56(3), 297–305.
- 693 <https://doi.org/10.1007/s11434-010-4209-x>
- 694 Wotton, R.S., Preston, T.M., 2005. Surface Films: Areas of Water Bodies That Are Often Overlooked.
- 695 *Bioscience* 55(2), 137–145. [https://doi.org/10.1641/0006-3568\(2005\)055\[0137:SFAOWB\]2.0.CO](https://doi.org/10.1641/0006-3568(2005)055[0137:SFAOWB]2.0.CO)
- 696 Wurl, O., Wurl, E., Miller, L.A., Johnson, K., Vagle, S., 2011. Formation and global distribution of
- 697 sea-surface microlayers. *Biogeosciences* 8(1), 121–135. <https://doi.org/10.5194/bg-8-121-2011>
- 698 Wurl, O., Holmes, M., 2008. The gelatinous nature of the sea-surface microlayer. *Mar. Chem.*
- 699 110(1–2), 89–97. <https://doi.org/10.1016/j.marchem.2008.02.009>
- 700 Yamashita, Y., Hashihama, F., Saito, H., Fukuda, H., Ogawa, H., 2017. Factors controlling the
- 701 geographical distribution of fluorescent dissolved organic matter in the surface waters of the
- 702 Pacific Ocean. *Limnol. Oceanogr.* 62(6), 2360–2374. <https://doi.org/10.1002/lno.10570>
- 703 Yamashita, Y., 2004. In situ production of chromophoric dissolved organic matter in coastal
- 704 environments. *Geophys. Res. Lett.* 31(14), 189–207. <https://doi.org/10.1029/2004GL019734>
- 705 Yang, L., Zhang, J., Yang, G.P., 2020. Mixing behavior, biological and photolytic degradation of
- 706 dissolved organic matter in the East China Sea and the Yellow Sea. *Sci. Total Environ.* 762(6),
- 707 143164. <https://doi.org/10.1016/j.scitotenv.2020.143164>
- 708 Yang, L., Zhuang, W., Chen, C.A., Wang, B., Kuo, F., 2017. Unveiling the transformation and
- 709 bioavailability of dissolved organic matter in contrasting hydrothermal vents using fluorescence
- 710 EEM-PARAFAC. *Water Res.* 111(Mar. 15), 195–203.
- 711 <https://doi.org/10.1016/j.watres.2017.01.001>
- 712 Zepp, R.G., Sheldon, W.M., Moran, M.A., 2004. Dissolved organic fluorophores in southeastern US
- 713 coastal waters: correction method for eliminating Rayleigh and Raman scattering peaks in



- 714 excitation–emission matrices. Mar. Chem. 89(1), 15–36.
- 715 <https://doi.org/10.1016/j.marchem.2004.02.006>
- 716 Zhu, W.Z., Yang, G., Zhang, H., 2017. Photochemical behavior of dissolved and colloidal organic
- 717 matter in estuarine and oceanic waters. Sci. Total Environ. s607–608(Dec. 31), 214–224.
- 718 <https://doi.org/10.1016/j.scitotenv.2017.06.163>



**Table 1** Spectral characteristics of the four fluorescent components identified by the PARAFAC

modal in this study, compared with those previously identified.

Component	$E_{x_{max}}$ (nm)	$E_{m_{max}}$ (nm)	Coble (1996)	Comparison with other studies using PARAFAC	Description and probable source
C1	345	455	peak C 320-360/42 0-480	Osburn et al. (2012)	Terrestrial-like humic substances
C2	255	375 (310)	peak A 230-260/380 -460	Stedmon et al. (2003)	Tyrosine-like substances
C3	315	385	peak M 290-310/370 -420	Stedmon and Markager (2005)	Marine humic-like substances (biological degradation)
C4	280	335	peak T 270-280/340 -350	Coble (1996)	Tryptophan-like; Non-Humic-like; Biological production in the water column



**Table 2** Average temperature, salinity, wind speed, CDOM  $a(254)$ , DOC, Chlorophyll- $a$  (Chl- $a$ ), dissolved oxygen (DO),  $S_{275-295}$ ,  $S_R$ , and  $SUVA_{254}$  of the SSW and SML in the BS, YS and ECS during spring, summer, autumn, and winter.

	Water layer	Spring		Summer		Autumn		Winter	
		mean	SD	mean	SD	mean	SD	mean	SD
Temperature ( $^{\circ}\text{C}$ )	SSW	14.0	4.91	24.0	3.66	13.7	2.69	14.0	5.23
Salinity	SSW	32.5	1.92	31.7	2.17	30.7	1.10	32.7	1.41
Wind Speed ( $\text{m s}^{-1}$ )	SSW	5.98	2.86	5.47	2.51	7.30	3.82	6.09	2.52
DO ( $\text{mg L}^{-1}$ )	SSW	6.44	0.85	7.57	1.07	7.49	0.51	8.32	0.99
Chl- $a$ ( $\mu\text{g L}^{-1}$ )	SSW	1.26	2.38	1.13	1.48	0.74	0.36	0.42	0.25
	SML	1.63	3.66	1.28	1.13	0.61	0.29	no data	
DOC ( $\mu\text{mol L}^{-1}$ )	SSW	91.3	25.7	109.4	33.55	151.2	83.8	88.4	22.51
	SML	132.9	77.4	145.7	49.8	146	33.5	131.3	91.1
$a(254)$ ( $\text{m}^{-1}$ )	SSW	3.20	2.49	3.10	1.34	5.21	1.84	2.52	1.26
	SML	3.70	1.98	4.05	1.66	5.51	1.82	4.74	2.50
$S_{275-295}$ ( $\text{nm}^{-1}$ )	SSW	0.0201	0.0049	0.0188	0.0035	0.0214	0.0075	0.0207	0.0068
	SML	0.0222	0.0073	0.0178	0.0021	0.0207	0.0067	0.021	0.0055
$S_R$	SSW	1.723	1.026	1.731	1.557	1.493	1.312	1.521	0.52
	SML	1.095	0.218	1.361	0.296	1.357	0.772	1.416	0.214
$SUVA_{254}$ ( $\text{L mg}^{-1} \text{C}^{-1} \text{m}^{-1}$ )	SSW	2.067	0.664	2.244	0.671	3.008	0.949	3.008	0.949
	SML	1.911	0.768	1.951	0.359	3.196	1.126	2.992	1.034



**Table 3** Correlation coefficients between EF of DOM optical properties, Chl-*a*, DOC, PO<sub>4</sub><sup>3-</sup>, NO<sub>3</sub><sup>-</sup>, NO<sub>2</sub><sup>-</sup>, SiO<sub>3</sub><sup>2-</sup>, Cyanobacteria, Picophytoplankton, Bacterial abundance.

	EF of a(254)	EF of DOC	EF of Chl- <i>a</i>	Ef of C1	EF of C2	EF of C3	EF of C4	EF of PO <sub>4</sub> <sup>3-</sup>	EF of NO <sub>3</sub> <sup>-</sup>	EF of NO <sub>2</sub> <sup>-</sup>	EF of SiO <sub>3</sub> <sup>2-</sup>	EF of Cyanobacteria	EF of picophytoplankton
EF of DOC	0.185												
EF of Chl- <i>a</i>	0.092	0.021											
Ef of C1	<b>.336**</b>	0.047	-0.119										
EF of C2	0.163	0.073	-0.017	<b>.635**</b>									
EF of C3	<b>.413**</b>	0.179	-0.096	<b>.907**</b>	<b>.557**</b>								
EF of C4	<b>.319**</b>	0.021	0.011	<b>.574**</b>	<b>.368**</b>	<b>.628**</b>							
EF of PO <sub>4</sub> <sup>3-</sup>	0.129	0.267	<b>.319*</b>	0.131	-0.037	0.139	0.087						
EF of NO <sub>3</sub> <sup>-</sup>	-0.065	-0.054	0.235	-0.037	-0.044	-0.027	-0.053	0.26					
EF of NO <sub>2</sub> <sup>-</sup>	0.15	0.208	<b>.307*</b>	0.142	-0.017	0.192	0.035	<b>.571**</b>	0.271				
EF of SiO <sub>3</sub> <sup>2-</sup>	<b>.634*</b>	0.004	0.074	0.122	-0.101	0.305	0.151	0.205	-0.118	-0.141			
EF of Cyanobacteria	0.091	-0.017	0.028	-0.027	-0.105	-0.047	-0.052	0.218	0.027	<b>.755**</b>	-0.286		
EF of Picophytoplankton	<b>.347**</b>	0.0281	0.252	-0.067	-0.082	-0.077	0.025	0.218	-0.08	0.113	-0.327	0.081	
EF of Bacterial abundance	-0.036	-0.069	-0.063	-0.061	0.004	0.014	-0.093	-0.12	-0.026	-0.073	-0.099	<b>.730**</b>	-0.064

\*\* Correlation is significant at the 0.01 level (two-tailed)

\* Correlation is significant at the 0.05 level (two-tailed)